Finite Element Analysis of Fretting Fatigue of Bolted Joints

Aidy Ali, M. K. Faidzi, M. H., Khairul H. Kamarudin, M. R. Saad

Abstract*: In this study, a simulation is conducted to determine the stress distribution near the contact surface of the bolted joints and its interactions by Solidwork and ANSYS workbench as fretting fatigue is frequently being described as the main reason for bolts' failure. The simulation result is compared with well published works, and it showed a strong in agreement. The bolt holes are is the most critical part and likely to fail rapidly during the time cycle compared to other parts.

Index Terms: Fatigue simulation, FEM.

I. INTRODUCTION

Bolted joints are one of the most common elements in construction especially in automotive engineering components and machine design. It consists of fasteners which act to capture and join the other parts, which are secured with the mating of screw threads. There are several advantages and disadvantages known of bolted joint. It is easy to disassemble and not sensitive to the parent material's condition. However, process of drilling the holes will cause crack propagation in a period of time to cause fatigue failure which can lead to plane crash as reported in [1] and bridge collapse which also caused by tensile stress and environment corrosion [2]. In this present study, the fretting fatigue of bolted joints is analyse using ANSYS AUTODYN simulation software. The study that could help and related to this work can be read in [1-28]

II. SIMULATION PROCEDURES

ANSYS AUTODYN is used as prediction of fretting fatigue mechanism of bolted joints by using Finite Elements (FE) simulation method. It is obtained through modeling and simulating the bolted joints.

A. Modeling Layout

The bolt is modeled using Solidwork software as shown in Fig. 1. A 3D model is created which is made up from 2024-T3 aluminium alloy for the joint and stainless steel for the bolt.

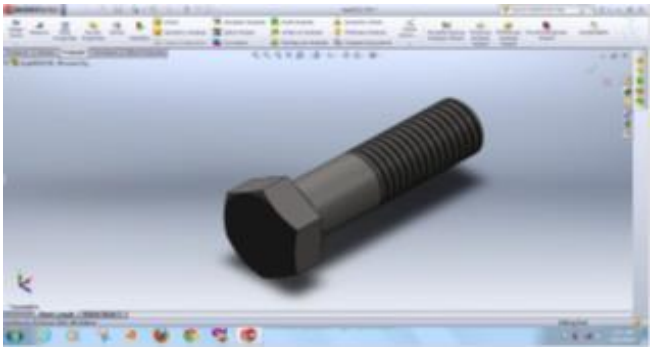

Fig. 1: Bolt modeled by Solidwork

B. Modeling Process

The model of bolted joint is drawn using Solidwork software according to previous study by [4] as illustrated in Fig. 2 and 3. The simulation of finite element analysis of fretting fatigue of bolted joint is modeled using the part modeler in ANSYS AUTODYN software.

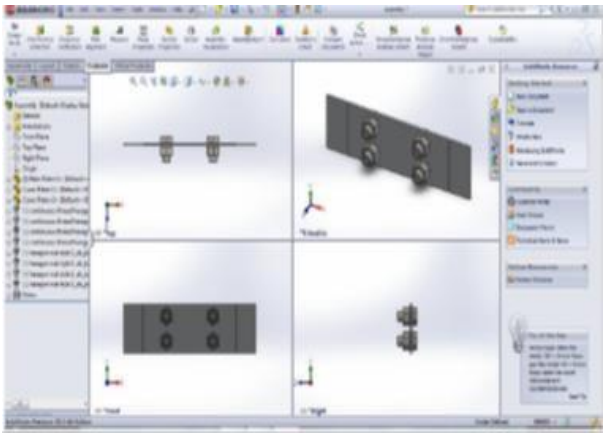

Fig. 2: Bolted joint in Solidwork assembly

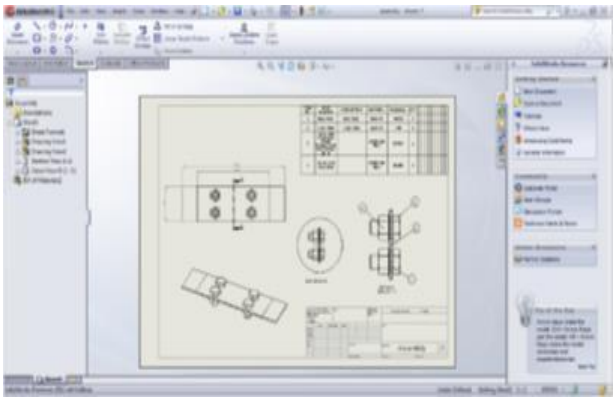

Fig. 3: Bolted joint in Solidwork drawing

Revised Manuscript Received on February 11, 2019.

Aidy Ali, Department of Mechanical Engineering, Faculty of Engineering, Universiti Pertahanan Nasional Malaysia (UPNM), Sg. Besi Camp, Kuala Lumpur, Malaysia.

M. K. Faidzi, Department of Mechanical Engineering, Faculty of Engineering, Universiti Pertahanan Nasional Malaysia (UPNM), Sg. Besi Camp, Kuala Lumpur, Malaysia.

Khairul H. Kamarudin, Department of Mechanical Engineering, Faculty of Engineering, Universiti Pertahanan Nasional Malaysia (UPNM), Sg. Besi Camp, Kuala Lumpur, Malaysia.

M. R. Saad, Department of Mechanical Engineering, Faculty of Engineering, Universiti Pertahanan Nasional Malaysia (UPNM), Sg. Besi Camp, Kuala Lumpur, Malaysia.

C. *Meshing Process*

Fig. 4 shows the meshing setup for the bolted joints model in ANSYS AUTODYN. It is evident that the finer the mesh, the result will be more accurate. The generated mesh depends on these factors which are created geometry, active mesh options, mesh control, and global element size and mesh tolerance.

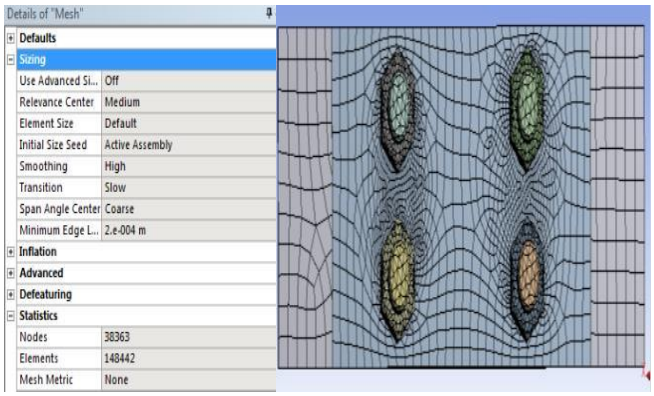

Fig. 4: Meshing setup for the bolted joints model in ANSYS AUTODYN

III. RESULTS AND DISCUSSION

A. Concentration of Area Plate Deformation

Different result for bolted joints model is obtained since each of the material has different hardness and toughness. The concentration area on the back surface of the bolted joint model shows the area that experiences the deformation after certain force is put. Fig. 5 shows that the deformation did not occur while the maximum deformation occurred on the main plate 1 with value of 1.6249 mm. Meanwhile, for Fig. 6-8 each axis shows that the deformation occurred mostly at z-axis with value of 0.921 mm. Table 1 displays the value of directional deformation for each axis.

Table 1: Directional deformation for each axis of bolted joints model

Axis	*x*	*y*	*z*	Total
Value (mm)	0.164	0.239	0.921	1.625
Maximum occurring	Main plate 1	Main plate 1	Main plate 1	Main plate 1
Minimum occurring	Main plate 1	Main plate 1	Head bolt	Main plate 1

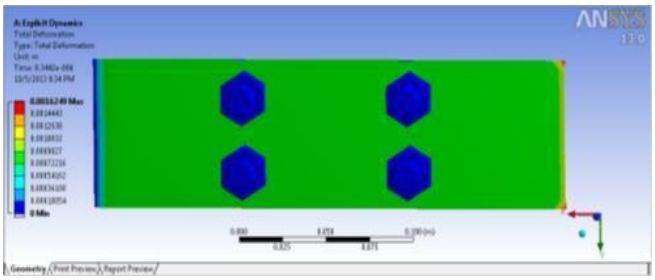

Fig. 5: Total deformation of bolted joints model

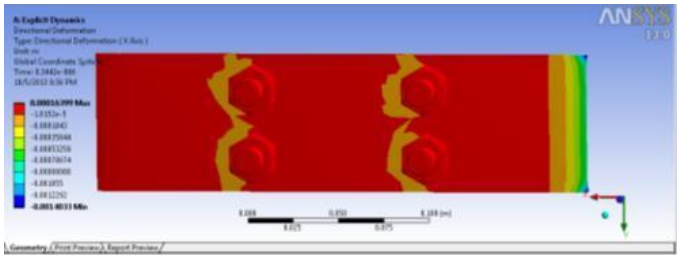

Fig. 6: Directional deformation towards *x*-axis

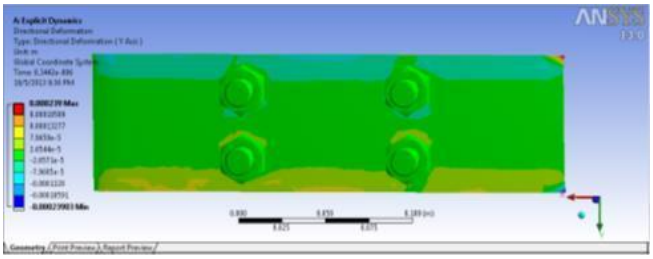

Fig. 7: Directional deformation towards *y*-axis

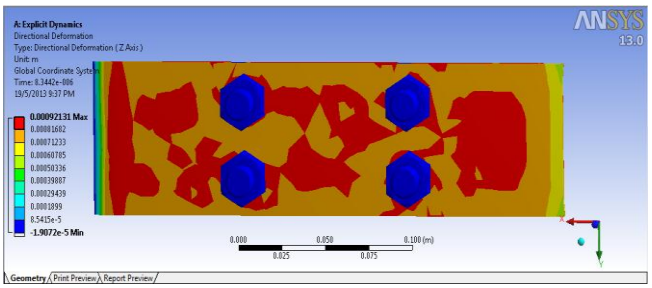

Fig. 8: Directional deformation towards *z*-axis

B. Concentration Area of Velocity

The concentration area of velocity refers to the area that most of the velocity area that acts on the bolted joints model. Fig. 9 shows the total velocity is 262.1 m/s which occurred at main plate 1. The maximum directional velocity occurred on the cover plate 1 with 100.54 m/s compared to *x*- and *y*-axis as shown in Fig. 10-12. Table 2 shows the velocity of directional deformation for each axis.

Table 2: Directional velocity for each axis of bolted joints model

Axis	*x*	*y*	*z*	Total
Velocity (m/s)	28.03	89.68	100.54	262.1
Maximum occurring	Main plate 1	Main plate 1	Main plate 1	Main plate 1
Minimum occurring	Main plate 1	Main plate 1	Cover plate 1	Main plate 1

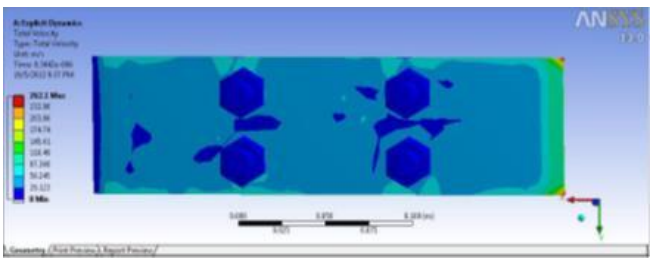

Fig. 9: Total velocity of bolted joints model

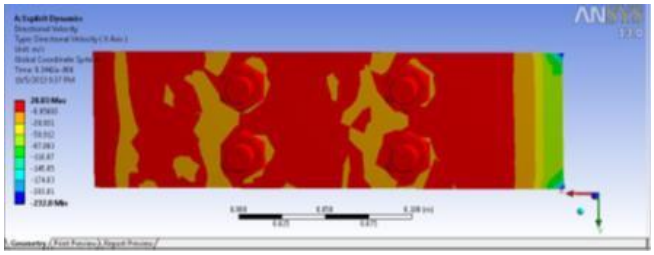

Fig. 10: Directional velocity of bolted joints model towards *x*-axis

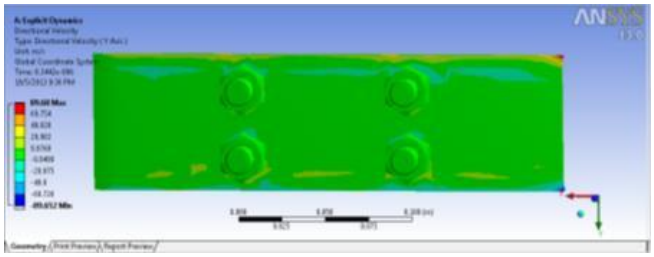

Fig. 11: Directional velocity of bolted joints model towards *y*-axis

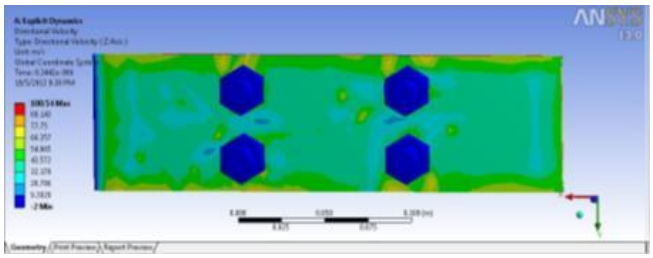

Fig. 12: Directional velocity of bolted joints model towards *z*-axis

C. Concentration Area of Acceleration

Concentration area of acceleration is referring to the area that acceleration occurred the most on the bolted joints model. Fig. 13 shows that total acceleration is 5.0347 x 107 m/s^2 which occurred mainly on main plate 1. Fig. 14-16 show the maximum directional acceleration occurred at z-axis on main plate 1 with value of 4.8432 x 107 m/s^2 compared to x- and y-axis which is displayed in Table 3.

Table 3: Directional acceleration for each axis of bolted joints model

Axis	*x*	*y*	*z*	Total
Acceleration (x 10^7 m/s^2)	3.112	3.8757	4.8432	5.0347
Maximum occurring	Main plate 1	Main plate 1	Main plate 1	Main plate 1
Minimum occurring	Main plate 1	Main plate 1	Main plate 1	Main plate 1

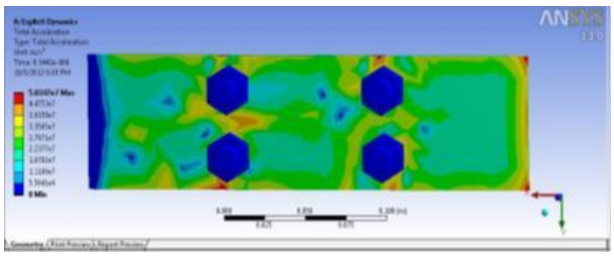

Fig. 13: Total acceleration of bolted joints model

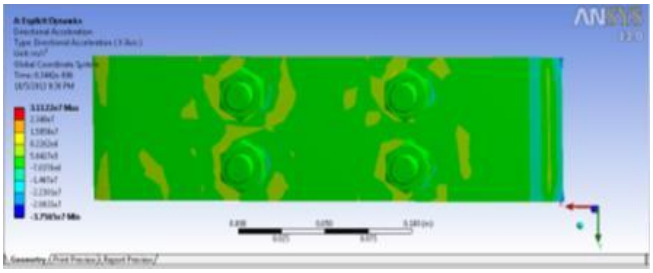

Fig. 14: Directional acceleration of bolted joints model towards *x*-axis

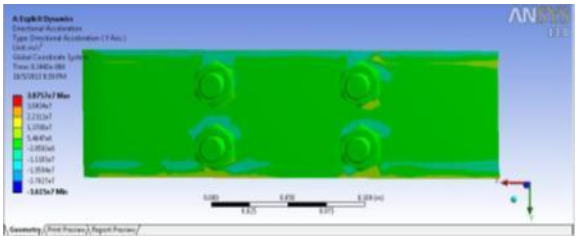

Fig. 15: Directional acceleration of bolted joints model towards *y*-axis

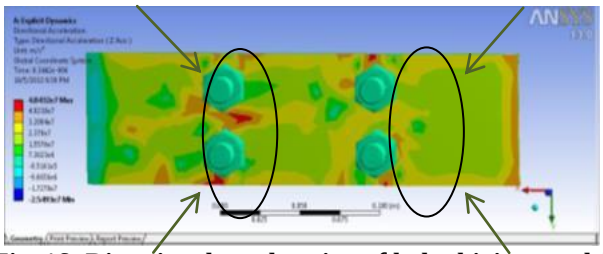

Fig. 16: Directional acceleration of bolted joints model towards *z*-axis

D. Concentration Area of Stress

ANSYS analysis shows that the maximum and minimum normal stress occurred on the *x*- and *z*-axis with value of 294.4 and 73.89 MPa respectively as shown in Fig. 17 and 18. Meanwhile, Table 4 shows the overall results for each plane on bolted joints model.

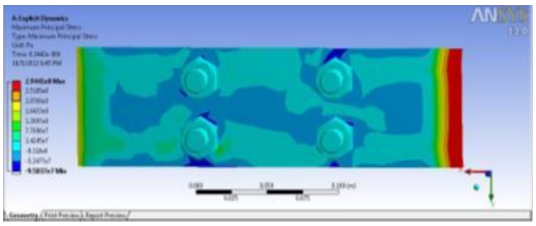

Fig. 17: Concentration area of maximum normal stress towards *x*-axis

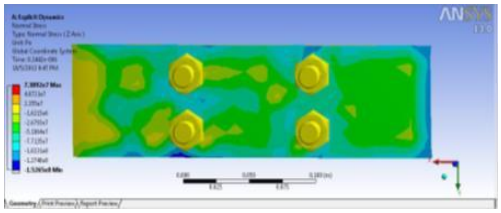

Fig. 18: Concentration area of minimum normal stress towards *z*-axis

Table 4: Overall stress respective to plane

Axis	*x*	*y*	*z*
Value (MPa)	294.4	116.8	73.89
Maximum occurring	Main plate 1	Main plate 1	Main plate 1
Minimum occurring	Main plate 1	Main plate 1	Main plate 1

Using the stresses value of *xyz* components in Table 4, the Von Mises stress can be written as

$$\sigma' = 1/\sqrt{2}[(\sigma_x - \sigma_y)^2 + (\sigma_y - \sigma_z)^2 + (\sigma_z - \sigma_x)^2 + 6(\tau_{xy}^2 + \tau_{yz}^2 + \tau_{xz}^2]^{1/2} \quad (1)$$

$$\sigma' = 1/\sqrt{2}[(177.56)^2 + (42.96)^2 + (-220.52)^2 + 6(41.37^2 + 46.21^2 + 58.66^2)]^{1/2}$$

$$\sigma' = 250.73 \text{ MPa}$$

Result obtained from the simulation for normal stress (294.41 MPa) is higher compared to Von Mises stress (250.73 MPa). Von Mises stress represent the equivalent stress.

$$\text{Stress amplitude, } \sigma_a = \frac{\sigma_{max} - \sigma_{min}}{2} \quad (2)$$

$$\sigma_a = \frac{294.41 - (-95.84)}{2}$$

$$\sigma_a = 195.13 \text{ MPa}$$

In general, the simulation results show that most vulnerable areas for the occurrence of fretting fatigue are at the bolts' holes. It is known that bolts' holes area are the most critical part in bolted joints model as illustrated in Fig. 19. This result is similar with the previous research that has been conducted experimentally. Fatigue crack growth usually starts on the surface at a point of stress concentration such as bolt holes. Fatigue cracks initiated at the outside of the zone weakened by the bolt holes at the interface contact surfaces between the main plate and cover plate.

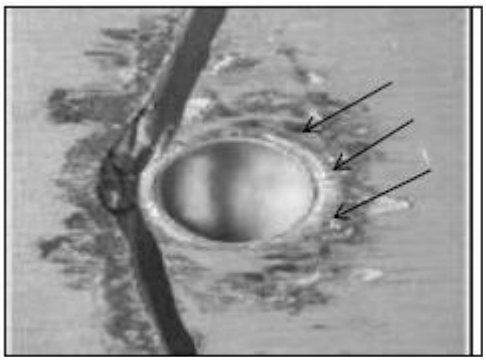

(a)

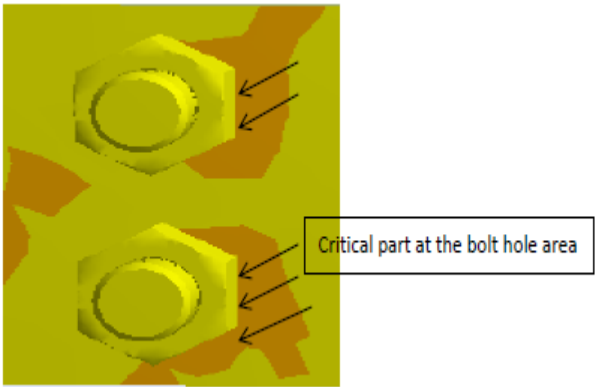

(b)

Fig. 19: Critical point at bolts holes (a) Experimental by [4] (b) simulation prediction

IV. CONCLUSION

From the simulation results, total stress amplitude that acted on the bolted joints model at time 10000 cycles is 195.13 MPa. The result is compared with study proposed by [3], which recorded 150 MPa. Thus, the percentage error is 23.12% which is considerably high. A high error percentage is contributed by factors such as meshing setup and inaccurate value of mechanical properties used. The critical area was successfully map and predicted using simulation.

REFERENCES

1. National Transportation Safety Board, Aircraft accident report: Apache Airlines Inc. DeHavilland DH-104-7AXC, N4922V. 1971, Available: https://www.ntsb.gov/investigations/AccidentReports/Reports/AAR7219.pdf.
2. C. Rose, "The collapse of the Silver Bridge," West Virginia Historical Society Quarterly, 15(4), 2001, pp. 1.
3. B. Atzori, P. Lazzarin, and M. Quaresimin, "A re-analysis on fatigue data of aluminium alloy bolted joints," International Journal Fatigue, 19(7), 1997, pp. 579-588.
4. H. R. Maleki and B. Abazadeh, "Fretting Fatigue behavior of bolted single lap joints of aluminum alloys," World Academy of Science, Engineering and Technology, 6(8), 2012, pp. 1509-1511.
5. K. Rassiah, M. M. H. M. Ahmad, and A. Ali, "Mechanical properties of laminated bamboo strips from Gigantochloa Scortechinii/polyester composites," Materials and Design, 57, 2014, pp. 551-559.
6. K. A. Mohammad, M. S. Salit, E. S. Zainudin, N. I. Zahari, and A. Ali, "Fatigue life prediction of austenitic type 316L stainless steel using ABAQUS," Advanced Materials Research, 911, 2014, pp. 59-462.
7. M. Sivarao, A. Ali, and L. S. Teng, "Enhanced tensile properties of stone wool fiber-reinforced high density polyethylene (HDPE) composites," Materials Testing, 56(2), 2014, pp. 150-154.
8. M. S. Salwani, B. B. Sahari, A. Ali, and A. A. Nuraini, "The effect of automotive side member filling on car frontal impact performance," Journal of Mechanical Engineering and Sciences, 6, 2014, pp. 873-880.
9. K. Rassiah, M. M. M. Ahmad, A. Ali, and H. Sihombing, "The effect of bamboo strip on the impact and hardness performances of unsaturated polyester composites," Journal of Applied Science and Agriculture, 10(8), 2015, pp. 8-12.
10. K. Rassiah, M. M. H. M. Ahmad, A. Ali, and M. M. Tamizi, "The influence of laminated layer and thickness gigantochloa scortechinii bamboo strips on mechanical performance of unsaturated polyester composites," Life Science Journal, 12(2), 2015, pp. 182-188.
11. K. Rassiah, M. M. H. M. Ahmad, and A. Ali, "Ballistic impact performance of the layered and laminated composites: A reviews," Pertanika Journal Science and Technology, 23(2), 2015, pp. 177-185.
12. M. S. Salwani, A. Ali, B. B. Sahari, and A. A. Nuraini, "Effect of automotive side member materials on the head injury criteria (HIC) and ches severity index (CSI) of adult passenger," International Journal of

Engineering and Technologies, 7, 2016, pp. 47-59.
13. M. Y. Soleha, K. K. Ong, W. Y. W. M. Zin, A. Mansor, F. Anwar, I. N. Azowa, S. A. S. M. Shafiq, A. Shah, N. Aisyah, A. Aidy, K. A. K. Z., and C. C. Teoh, "Characterization of raw and thermally treated alum sludge," Key Engineering Materials, 701, 2016, pp. 138-142.
14. S. Subramonian, A. Ali, M. Amran, L. D. Sivakumar, S. Salleh, and A. Rajaizam, "Effect of fiber loading on the mechanical properties of bagasse fiber–reinforced polypropylene composites," Advances in Mechanical Engineering, 8(8), 2016, pp. 1–5.
15. K. Rassiah, M. M. H. M. Ahmad, and A. Ali, "Effect on mechanical properties of rice husk/e-glass polypropylene hybrid composites using sodium hydroxide (NaOH)," Journal of Advances in Technology and Engineering Research, 2(4), 2016, pp. 105-112.
16. M. J. Suriani, A. Ali, A. Khalina, and S. M. Sapuan, "Fatigue life estimation of kenaf reinforced composite materials by non-destructive techniques," Universal Journal of Materials Science, 4(4), 2016, pp. 88-96.
17. S. A. Ibraheem, S. S. Sreenivasan, K. Abdan, S. A. Sulaiman, A. Ali, and D. L. A. A. Majid, "The effects of combined chemical treatments on the mechanical properties of three grades of sisal," BioResources, 11(4), 2016, pp. 8968-8980.
18. A. Ali, K. Rassiah, F. Othman, L. H. Pueh, T. T. Earn, M. S. Hazin, and M. M. H. M. Ahmad, "Fatigue and fracture properties of laminated bamboo strips from gigantochloa scortechinii / polyester composites," BioResources, 11(4), 2016, pp. 9142-9153.
19. M. Sivarao, A. Ali, M. Amran, L. D. Sivakumar, S. Salleh, and A. Rajaizam, "Performance evaluation of reworked weld joints," International Journal of Engineering and Technologies, 9, 2016, pp. 47-59.
20. K. Rassiah and A. Ali, "A study on mechanical behaviour of surface modified rice husk/polypropylene composite using sodium hydroxide," International Journal of Engineering and Technologies, 8, 2016, pp. 72-82.
21. N. A. Halim, A. Ali, Z. H. Z. Abidin, A. B. Ahmad, and A. Z. Sulaiman, "Thermal analysis of organically modified Ca montmorillonite using DSC and TSC techniques," Journal of Thermal Analysis and Calorimetry, 128(1), 2017, pp. 135-140.
22. K. Rassiah, M. M. H. M. Ahmad, A. Ali, A. H. Abdullah, and S. Nagapan, "Mechanical properties of layered laminated woven bamboo gigantochloa scortechinii / epoxy composites," Journal of Polymer and Environment, 26(4), 2018, pp. 1328-1342.
23. A. Ali , W. K. Ng, F. Arifin, K. Rassiah, F. Othman, M. S. Hazin, and M. M. H. M. Ahmad, "Development and mechanical characterization of green bamboo composites," AIP Conference Proceedings, 1930, 2018, pp. 1-6.
24. A. Ali, N. W. Kuan, F. Arifin, K. Rassiah, F. Othman, S. Hazin, and M. H. M. Ahmad, "Fracture properties of hybrid woven bamboo/woven e-glass fiber composites," International Journal of Structural Integrity, 9(4), 2018, pp. 491-519.
25. A. Ali, R. Adawiyah, K. Rassiah, W. K. Ng, F. Arifin, F. Othman, M. S. Hazin, M. K. Faidzi, M. F. Abdullah, and M. M. H. M. Ahmad, "Ballisctic impact properties of woven bamboo-woven e glass-unsaturated polyester hybrid composites," Defense Technology, 9(4), 2018, pp. 491-519.
26. M. K. F. M. Paudzi, M. F. Abdullah, and A. Ali, "Fatigue analysis of hybrid composites of kenaf/kevlar fibre reinforced epoxy composites," Jurnal Kejuruteraan, 1(7), 2018, pp. 1-8.
27. M. K. Faidzi, A. K. Hamizi, M. F. Abdullah, M. A. Aliimran, K. Z. K. Ahmad, R. N. Othman, and A. Ali, "Fatigue crack growth behaviour of sandwiched metal panel of aluminium and mild steel under constant amplitude loading," International Journal of Engineering and Technology UAE, 7(4.33), 2018, pp. 362-366.
28. A. Ali, B. B. Sahari, and M. S. Salwani, "Simple durability programming integrated with LSDYNA for automotive applications," International Journal of Engineering and Technology UAE, 7(4.33), 2018, pp. 299-306.